DISCLAIMER

SRC Technical Notes are informal memos intended for internal communication and documentation of work in progress. These notes are not necessarily definitive and have not undergone a pre-publication review. If you rely on this note for purposes other than its intended use, you assume all risk associated with such use.

University of Wisconsin-Synchrotron Radiation Center TECHNICAL NOTE	**File No.** **SRC-209**	**Page** 1 of 23
Subject: **A 2.1-GeV ring design for SRC**	**Author(s):** **R. A. Bosch**	
	Date: **October 14, 2004 revised October 5, 2006**	

A design for a twelve-sided 2.1-GeV electron storage ring is obtained. The design utilizes the combined-function magnet approach of the Max-IV design for 1.5-GeV and 3-GeV rings. The 2.1-GeV ring has an emittance of 1.5 nm-rad and circumference of 215 m, with twelve 5.5-m long straight sections.

With a 100-MHz radiofrequency (RF) system, an adequate Touschek current-lifetime product of ~3000 mA-hours is computed. The lifetime is not limited by the computed dynamic aperture.

Modeling of a passive fifth harmonic RF system suggests that a 100-MHz/500-MHz system may be successfully operated to increase the bunchlength and Touschek lifetime by a factor of four while suppressing typical parasitic coupled-bunch instabilities. For stable operation with ring currents up to 600 mA, microwave-instability simulations indicate that the reduced longitudinal broadband impedance should be less than 1.5 ohms.

The properties of the ring design suggest that a low-emittance 2.1-GeV ring with a circumference of 215 m is a feasible upgrade path for the Synchrotron Radiation Center.

1. Introduction

A new ring to serve the scientific needs of the SRC community is designed. The ring energy of 2.1 GeV will allow insertion devices to cover the desired photon energy range of 1–2000 eV [1]. Here we consider a ring design similar to the MAX-IV design for 1.5-GeV and 3-GeV rings [2]. The MAX-IV design incorporates combined-function magnets in a 12-sided ring of length 287 m, with long straight sections of length 4.6 m. Our desired 2.1 GeV ring energy is 30% lower than the 3-GeV energy of the higher-energy MAX-IV ring. This allowed us to design a shorter 12-sided ring with circumference of 215 m that incorporates longer straight sections of 5.5 m length, with nearly the same emittance as the MAX-IV 3-GeV design. The low emittance is expected to allow the usage of small-aperture magnets and small-gap insertion devices with a reasonable amount of horizontal-vertical coupling.

By using two families of sextupoles for chromaticity correction, we achieved a horizontal dynamic aperture (for energy deviations up to ±3% and ideal magnets) of [−10 mm, +6mm], which is 60% of the desired vacuum chamber horizontal aperture of [−10 mm, +10mm]. By adding a single family of harmonic sextupoles, the horizontal dynamic aperture was increased to [−20 mm, +10mm], with vertical dynamic aperture of ±3 mm exceeding the desired vertical vacuum chamber aperture of ±2 mm. Since reasonable magnetic field errors and misalignments have little effect on the MAX-IV dynamic aperture [2], we expect that the dynamic aperture of our design is sufficient.

Modeling of an RF system employing six 100-MHz cavities gives an adequate Touschek lifetime of 14 hours for a ring current of 200 mA. The computed dynamic aperture does not limit the lifetime. With the use of two passive 500-MHz cavities, the bunch length and Touschek lifetime are quadrupled while typical longitudinal parasitic coupled-bunch instabilities are suppressed. For stable operation with ring currents up to 600 mA, simulations of the microwave instability indicate that the reduced longitudinal broadband impedance should be smaller than 1.5 ohms.

2. Initial gross design

To produce a design using the MAD accelerator design code [3], we converted a MAX-IV lattice file obtained from MAXlab in the UTRANSPORT format of the DIMAD code [4]. Since MAD doesn't model combined-function quadrupole/sextupole magnets, each magnet of this type was modeled as a quadrupole with three equal-strength thin sextupoles at the ends and center. This approximation is expected to provide sufficient accuracy for chromaticity correction and dynamic aperture computations [5]. The MAX-IV lattice functions computed with MAD for a superperiod are shown in Fig. 1, while the MAD lattice file is in Appendix A. The MAX-IV superperiod contains 5 combined-function UNDIP bending magnets, flanked by MATDIP and SOFTDIP bending magnets. The SOFTDIP magnets have a weak dipole field to reduce the synchrotron radiation energy deposited on the long-straight-section vacuum tanks.

Since the MAX-IV design has been studied in detail for several years, we assume that the MAX-IV magnet field strengths are feasible at the design energy of 3 GeV. A given magnetic field has 40% more effect upon a 2.1-GeV electron, so we can obtain the same focusing and bending with a 30% decrease in magnet length. Alternatively, we can decrease the lengths of quadrupoles by a smaller degree and use the increase in feasible focusing strength to shorten the drift spaces.

Accordingly, we decreased quadrupole lengths and drift spaces by 20%, except for the long straight sections, which we increased from 4.6 m to 5.5 m to allow longer undulators or three of the 1.7-m insertion device modules favored by ESRF. The quadrupole focusing strengths per unit length ("K1" in MAD notation) were increased by 40%, giving no change in the B-field within the magnet gap. The thin sextupole strengths ("K2L" in MAD notation) were increased by 12%, corresponding to a 20% decrease

in combined-function magnet length with a 40% increase in sextupole strength per unit length; this also corresponds to no change in B-field. The MATDIP and SOFTDIP combined dipole/quadrupole bending magnet lengths were reduced by 30%, the bending angle was unchanged, and their quadrupole strengths-per-unit-length K1 were increased by 40%; corresponding to no change in B-field. To further shorten the ring, we reduced the number of UNDIP magnets (and associated drift spaces) from five to three. Their length was modified by (2.1/3)(5/3) = 1.23667, their bending angle was modified by 5/3, while their quadrupole strength per unit length was increased by 40%. Again, this corresponds to no change in B field within the magnet gap. The result of these modifications was an unstable lattice design whose magnetic fields are feasible under the assumption that those of MAX-IV are feasible.

To proceed, we examined the "unit cell" of this lattice, modeled with periodic boundary conditions. The unit cell contains a UNDIP bending magnet with horizontally defocusing quadrupole strength UNDIP[K1] and a horizontally focusing quadrupole QFUN. These two quadrupole strengths were modified so that the beta-functions and phase advance are comparable to those of a unit cell of MAXIV. The entire ring was then examined and found to be unstable. By changing the SS2 drift length from 0.4 m to 0.6 m, a stable ring with emittance of 3.8 nm-rad at 2.1 GeV was obtained. A further modification of the SS2 drift length to 0.7 m lowered the emittance to 2.38 nm-rad, with a ring circumference of 217 m.

We then modified the quadrupole strengths of MATDIP and UNDIP to achieve $\beta_x = 8$ m and $\beta_y = 2.6$ m in the center of the long straight sections. This β_y value is close to the ideal value of 2.75 m, which is one-half of the long straight section length. The value of β_x is larger to allow injection into a long straight section. The resulting lattice, whose emittance is 2.33 nm-rad, was designated AladdinIV_3. Its lattice functions are shown in Fig. 2, while Appendix B gives its MAD lattice file with sextupole settings that zero the chromaticity.

3. Matching for low emittance

Having achieved the gross properties desired, we used the matching capabilities of MAD to fine-tune the lattice design by varying quadrupole strengths and the lengths of two drift spaces. The matching routine constrains dispersion at the beginning and ends of the UNDIP bending magnets. It also constrains the beta-functions to specific values in the middle of the long straight sections and QFUN quadrupole centers. The β_y-values throughout the ring and near the middle of the superperiod were also constrained with inequalities. In MAD matching, the constraints are only applied at the ends of elements in the lattice file, and therefore a constraint such as $\beta_y < 20$ m does not preclude larger β_y-values from occurring in the middle of drift spaces, etc.

The numerical values to which the lattice functions were constrained were determined by trial and error. For a given set of constraint values, a lattice was obtained by matching. After examining the lattice's properties, new values of the constraints were tried. After several iterations, we obtained the MATCH4.MAD matching file shown in Appendix C. The lattice functions of the resulting "MATCH4" ring design are plotted in Fig. 3.

Figure 3 was plotted using MAD's SPLINE specification to show the lattice functions within lattice elements. Apparently the SPLINE feature doesn't work. By using the SPLIT command, we determined that β_x decreases to a minimum of 0.5 m in the UNDIP dipoles, while β_y increases to a maximum of 9.3 m in the middle UNDIP dipole and 10.1 m in the other two UNDIP dipoles. The horizontal dispersion decreases to 0.052 m in the middle UNDIP dipole and 0.030 m in the other two UNDIP dipoles.

For the MATCH4 lattice, the circumference is 215.13 m, 25% shorter than MAX-IV. The long straight section length is 5.5 m, 20% longer than MAXIV. The momentum compaction is 0.001066, 45% larger than MAX-IV. The emittance for 2.1-GeV operation is 1.468 nm-rad, which is 16% larger than the

emittance of MAX-IV for 3-GeV operation. The tunes are (22.591, 6.368), comparable to 215/287 times the MAXIV tunes of (26.60, 9.590).

The maximum β_x is 8.95 m; the maximum β_y is 17.53 m; the maximum horizontal dispersion is 0.136 m. Thus, a large 7% energy error would be required for the closed orbit to strike a vacuum chamber wall that is 10 mm horizontally displaced from the axis. The energy spread is 7.75×10^{-4}, the synchronous voltage is 231.42 kV, and the longitudinal radiation-damping time is 8.75 ms.

4. Sextupoles and dynamic aperture

By using the SD and QFUN sextupoles (with the QFM harmonic sextupole at zero), we zeroed the chromaticity. The resulting dynamic aperture in the middle of a 5.5-m long straight section, shown in Fig. 4, is smaller than the desired vacuum chamber size of 20 mm (horizontal) x 4 mm (vertical), where we use the MAX-IV vacuum chamber size as the "desired size". Using MAD's HCELL command, we determined the excitation of the QFM harmonic sextupole that zeros the derivative of horizontal tune with amplitude. The improved dynamic aperture with this sextupole setting is shown in Fig. 5. The MAD lattice file for this "MATCH4" lattice is given in Appendix D. The ML octupole inherited from the MAX-IV design is not used.

5. 100-MHz RF system

We consider operation with a 100.4-MHz RF system. For a 100.4-MHz RF system with voltage of 1.2 MV, the MATCH4 lattice's synchrotron frequency is 3.64 kHz, and the rms bunchlength is 10.774 mm. For 200 mA in 72 bunches with 1.5% emittance coupling, the Touschek lifetime determined by MAD is 29.7 hours. This is 70% longer than the MAX-IV Touschek lifetime computed by MAD for 2.1 GeV operation with a 100-MHz RF system with RF voltage of 1.2 MV, 200 mA in 95 bunches with 1.5% emittance coupling.

To estimate the effect of physical and dynamic apertures on the lifetime, we calculated the lifetime using the ZAP code [6] for the case where the horizontal physical half-aperture is 0.01 m throughout the ring. To adequately sample the lattice functions, ZAP was modified to use as many as 40,000 ring positions. We used a ZAP input file in which each drift space and dipole magnet is divided into ten pieces, while each quadrupole is divided into 20 pieces. For 200 mA in 72 bunches with 1.5% emittance coupling, the calculated Touschek lifetime for an RF voltage of 1.2 MV is 14.76 hour, giving a current-lifetime product of 2952 mA-hours.

For greater accuracy, ZAP was modified to use a lifetime formula that doesn't assume nonrelativistic electron velocities in the beam frame [7]. This computation gives a Touschek lifetime of 14.22 hours (for 200 mA in 72 bunches with 1.5% emittance coupling and RF voltage of 1.2 MV), with a current-lifetime product of 2844 mA-hour. For a physical half-aperture of 0.008 m, the lifetime is reduced 50% to 7.17 hours. With a physical half-aperture of 0.006 m, the lifetime is 2.95 hours, while a lifetime of 1.719 hours is computed for a physical half-aperture of 0.005 m. Losses to physical apertures occur at the locations of maximum horizontal dispersion.

The computed lifetime for a physical half-aperture of 0.01 m is unchanged if a larger dynamic aperture is specified, indicating that the computed dynamic aperture does not limit the lifetime. By specifying physical and dynamic apertures that are a factor of ten larger, ZAP computed the lifetime from the RF bucket as 39.7 hours, about 34% larger than the MAD computation in which ring locations are poorly sampled.

By using emittance coupling larger than 1.5% and/or a fifth-harmonic cavity for bunchlengthening, the Touschek lifetime may be increased. Since a lifetime of several hours suffices for top-up injection, the ring lifetime appears to be long enough.

6. Harmonic cavity modeling

Using a passive fifth harmonic RF cavity to lengthen the bunch is expected to increase the lifetime and the Landau damping of parasitic coupled-bunch instabilities. Successful harmonic-cavity operation may prevent the need for a longitudinal feedback system and increase the current threshold of microwave instability. However, Robinson instabilities must be avoided. We consider the use of six 100-MHz and two 500-MHz cavities with the same parameters and RF-coupling of MAXlab [8]. The parameters are shown in Appendix E.

The methods used for analytic predictions and simulations are described in Ref. [9] and [10]. According to Ref. [10], accurate simulations of Robinson and parasitic coupled bunch instabilities require ≥ 1000 macroparticles in the ring, while accurate simulations of microwave instability require ≥ 1000 macroparticles per bunch. To complete the microwave-instability simulations, we performed several simulations simultaneously by using the University of Wisconsin-Madison's CONDOR® pool for high-throughput computing. This pool performs computations by utilizing the otherwise idle time of networked workstations and personal computers [11].

Figure 6(a) shows analytic instability predictions without considering higher-order modes in the RF cavities. Several values of the ring current and harmonic-cavity-tuning angle are modeled. For currents of 360–600 mA, optimal bunchlengthening is predicted to be stable, increasing the bunchlength by a factor of four. At currents of 200–320 mA, the analytic modeling predicts that near-optimal bunchlengthening is stable, while optimal bunchlengthening is destabilized by Robinson instabilities.

Figure 6(b) shows results from simulating 1440 macroparticles for 500,000 turns (41 radiation-damping periods). For each simulation, the relative energy spread and number of lost macroparticles at the end of the simulation were recorded. An energy spread that exceeds the natural value by more than 10% is taken as a sign of instability. In Fig. 6(b), a circle is plotted when the energy spread at the end of a simulation exceeds the natural value by more than 10%, while a solid square is plotted when macroparticles are lost in a simulation. Lost macroparticles occur for parameters where instability is predicted in Fig. 6(a), consistent with their loss from instability. The simulations shown in Fig. 6(b) are in approximate agreement with the analytic modeling of Fig. 6(a).

Figure 7(a) shows analytic predictions where a parasitic higher-order mode (HOM) is considered with quality factor of 3000, resonant impedance of 10 kΩ, and resonant frequency of 0.9998605 GHz. The HOM properties are chosen to approximate a typical mode in a 100 MHz cavity with HOM damping. For the HOM, the analytic predictions consider a worst-case scenario where the mode's frequency maximally excites non-Robinson coupled-bunch instability. Figure 7(b) shows 500,000-turn simulations of 1440 macroparticles with a worst-case HOM frequency of 0.9998605 GHz, which equals 717 times the revolution frequency. Good agreement between analytic modeling and simulations is obtained. The analytic modeling and simulations both indicate that optimal bunchlengthening provides sufficient Landau damping to suppress the parasitic coupled-bunch instability from a typical HOM.

To study the effect of broadband impedance from the vacuum chamber, the microwave instability is considered for a HOM with quality factor of one and resonant angular frequency of c/b, where c is the speed of light and b is the vacuum chamber radius. An analytic prediction, described in Ref. [10], considers whether the negative-mass instability of a coasting beam can overcome Landau-damping resulting from the longitudinal velocity spread caused by the beam's energy spread, as in the ZAP code [6]. Figure 8(a) shows analytic predictions for a broadband HOM with quality factor of 1, resonant

impedance of 1712.5 Ω, and resonant frequency of 4.77 GHz. This HOM models reduced longitudinal broadband impedance $|Zp/p|$ of 0.5 Ω in a chamber with radius of 10 mm. Instability is predicted for sufficiently high ring current and low harmonic-cavity voltage.

Figure 8(b) shows results of 200,000-turn simulations of 4000 macroparticles/bunch. In these simulations, macroparticles are lost for high ring currents and low harmonic-cavity voltage, in rough agreement with the analytic model.

Figures 9–11 show modeling for reduced broadband impedances of 1 Ω, 1.5 Ω, and 2 Ω. Approximate agreement between the modeling and simulations is obtained.

Comparisons with Aladdin data indicate that microwave instability thresholds determined by simulations agree with experiment [10]. According to simulations of our 2.1-GeV ring design, optimally lengthened bunches are not affected by the microwave instability for ring currents up to 600 mA when the broadband impedance obeys $|Zp/p| \leq 1$ Ω. Stable double-hump bunches are not affected by the microwave instability for ring currents up to 600 mA when the broadband impedance obeys $|Zp/p| \leq 1.5$ Ω. Broadband impedance of this magnitude may be achieved with a vacuum chamber design similar to those of the light sources SOLEIL [12], SPEAR3 [13], SPRING8 [14], BESSY-II [15] and APS [16].

7. Summary

We have studied the "MATCH4" design for a 2.1-GeV ring with low emittance of 1.5 nm-rad and a fairly small circumference of 215 m. Twelve 5.5-m straight sections are provided — eleven for insertion devices and one for injection. The energy spread is 7.75×10^{-4}, the synchronous voltage is 231.42 kV, and the longitudinal radiation-damping time is 8.75 ms. With a ring current of 200 mA and 1.5% emittance coupling, a vacuum chamber half-width of 10 mm gives a Touschek lifetime of 14 hours with a 100-MHz RF system.

Modeling of a passive fifth harmonic RF system suggests that a 100-MHz/500-MHz system may be successfully operated to increase the bunchlength and Touschek lifetime by a factor of four while suppressing typical parasitic coupled-bunch instabilities. For stable operation with a ring current up to 600 mA, simulations of the microwave instability indicate that the reduced longitudinal broadband impedance $|Zp/p|$ should not exceed 1.5 Ω.

Assuming that construction of the MAX-IV magnets is feasible, the feasibility of the MATCH4 magnets was evaluated. If the MAX-IV magnet strengths are at the upper limit of feasibility, it may be necessary to lengthen the MATCH4 QFUN combined quadrupole/sextupole by 15%. It may also be necessary to lengthen the SD sextupole by 30%.

The properties of the MATCH4 lattice suggest that a low-emittance 2.1-GeV ring with a circumference of 215 m is a feasible upgrade path for the Synchrotron Radiation Center.

References

[1] M. A. Green, private communication (2003).

[2] H. Tarawneh, M. Eriksson, L-J. Lindgren and B. Anderberg, Nucl. Instrum. Methods Phys. Res., Sect. A 508, 480 (2003).

[3] H. Grote and F. C. Iselin, "The MAD Program (Methodical Accelerator Design) Version 8.1 User's Reference Manual," CERN/SL/90-13 (1990).

[4] R. V. Servrancks, K. L. Brown, L. Schachinger and D. Douglas, "Users Guide to the Program DIMAD," SLAC Report UC-28 (A), (May 1985).

[5] D. Einfeld, private communication (2004).

[6] M. S. Zisman, S. Chattopadhyay and J. J. Bisognano, "ZAP User's Manual," Lawrence Berkeley Laboratory Report No. LBL-21270, 1986.

[7] A. Piwinski, "The Touschek effect in strong focusing storage rings," Deutsches Elektronen-Synchrotron Report No. DESY 98-179, 1998, Eq. 48.

[8] R. A. Bosch, "Instability modeling for passive harmonic-cavity operation at MAXlab," Synchrotron Radiation Center Technical Note No. SRC-206 (2004).

[9] R. A. Bosch, K. J. Kleman and J. J. Bisognano, Phys. Rev. ST Accel Beams 4, 074401 (2001).

[10] R. A. Bosch, Phys. Rev. ST Accel Beams 8, 084401 (2005).

[11] Condor Team, University of Wisconsin-Madison, "Condor Version 6.6.7 Manual," Computer Sciences Department, University of Wisconsin-Madison, Madison, WI, 2004.

[12] R. Nagaoka, in *Proceedings of the 2004 European Particle Accelerator Conference, Lucerne, Switzerland* (in press).

[13] C. Limborg and J. Sebek, in *Proceedings of the 1999 Particle Accelerator Conference, New York, NY* (IEEE, Piscataway, NJ, 1999), p. 2361.

[14] T. Nakamura, in *Proceedings of the 1993 Particle Accelerator Conference, Washington, DC* (IEEE, Piscataway, NJ, 1993), p. 3464.

[15] S. Khan, in *Proceedings of the 1997 Particle Accelerator Conference, Vancouver, Canada* (IEEE, Piscataway, NJ, 1998), p. 1703.

[16] Y.-C. Chae, K. Harkay and X. Sun, in *Proceedings of the 2003 Particle Accelerator Conference, Portland, OR* (IEEE, Piscataway, NJ, 2003), p. 3014.

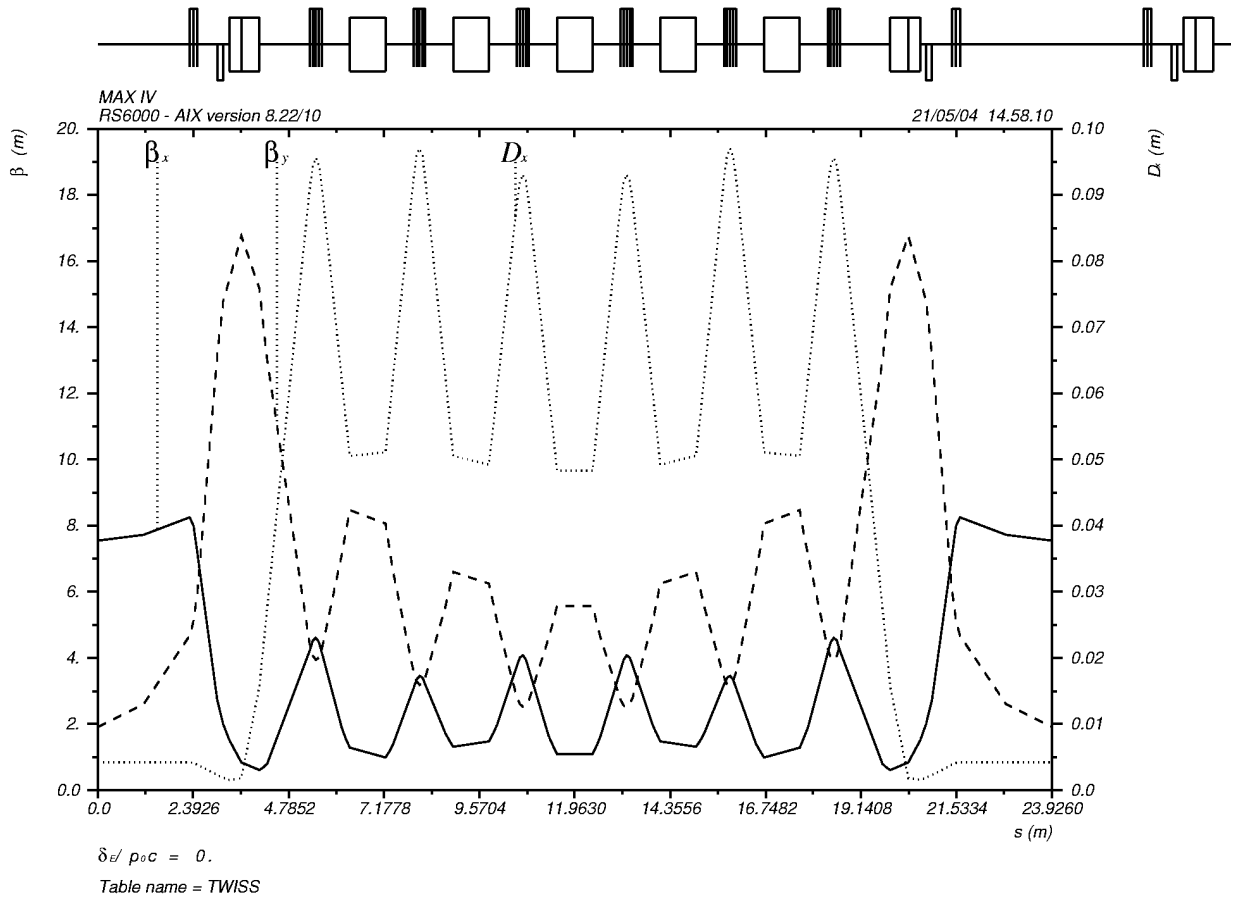

Figure 1. Lattice functions for one superperiod of the MAX-IV design.

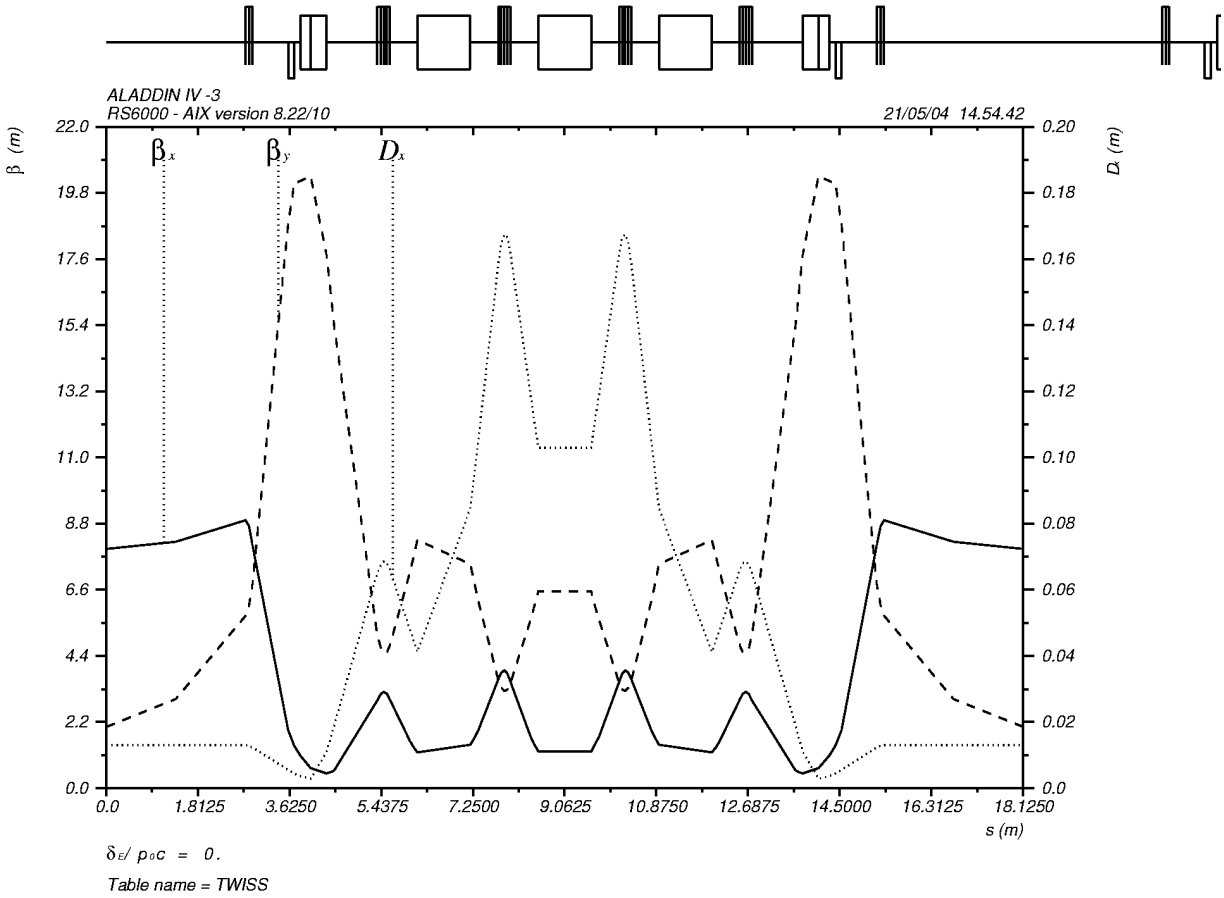

Figure 2. Lattice functions for one superperiod of the AladdinIV_3 lattice.

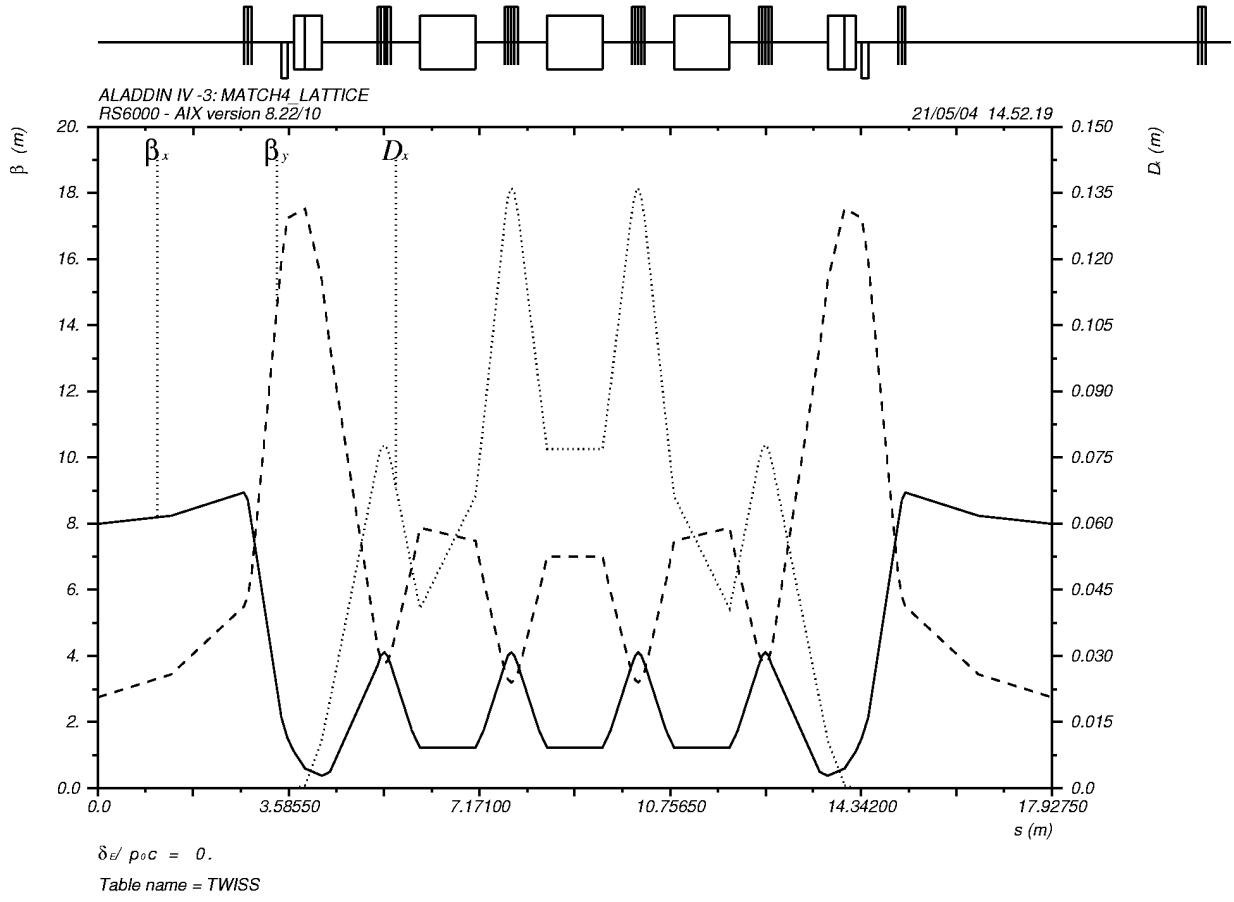

Figure 3. Lattice functions for one superperiod of the MATCH4 lattice

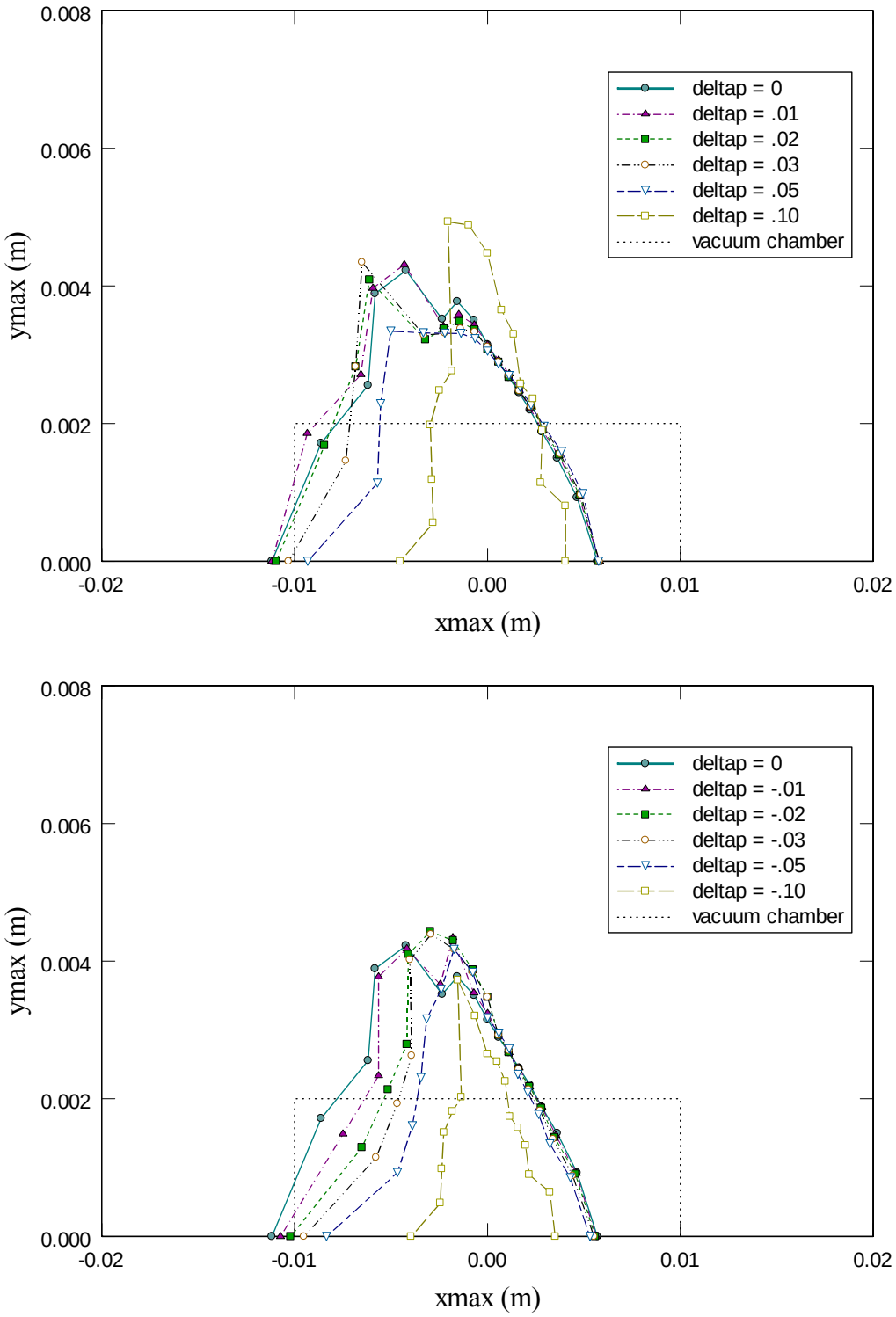

Figure 4. 1000-turn dynamic aperture computed by the MAD code for the MATCH4 lattice, with two sextupole families used for chromaticity correction. The dynamic aperture is shown for several values of "deltap," which is the relative momentum deviation.

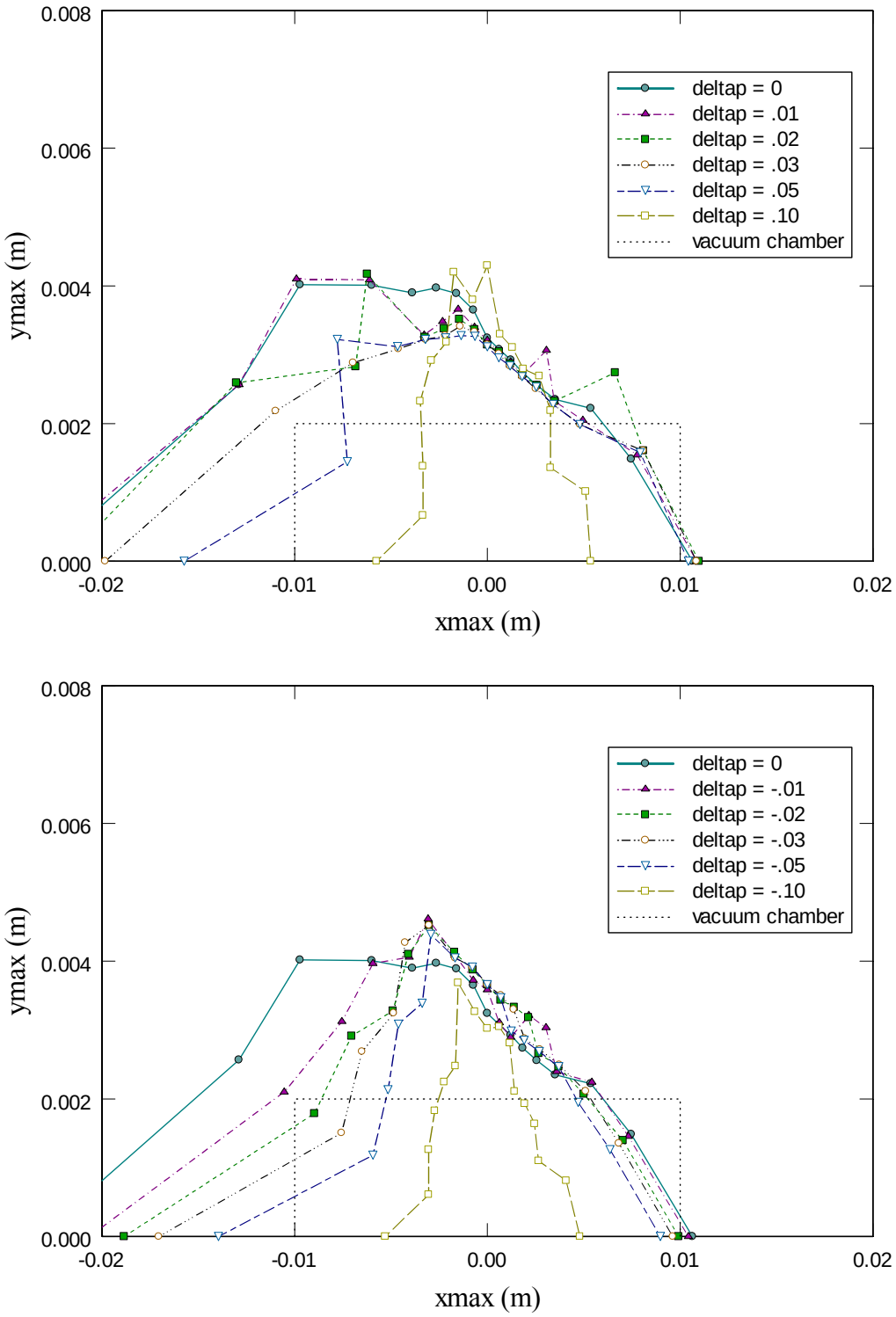

Figure 5. 1000-turn dynamic aperture of the MATCH4 lattice with two sextupole families used for chromaticity correction and one harmonic sextupole family used to zero the derivative of tune with respect to amplitude.

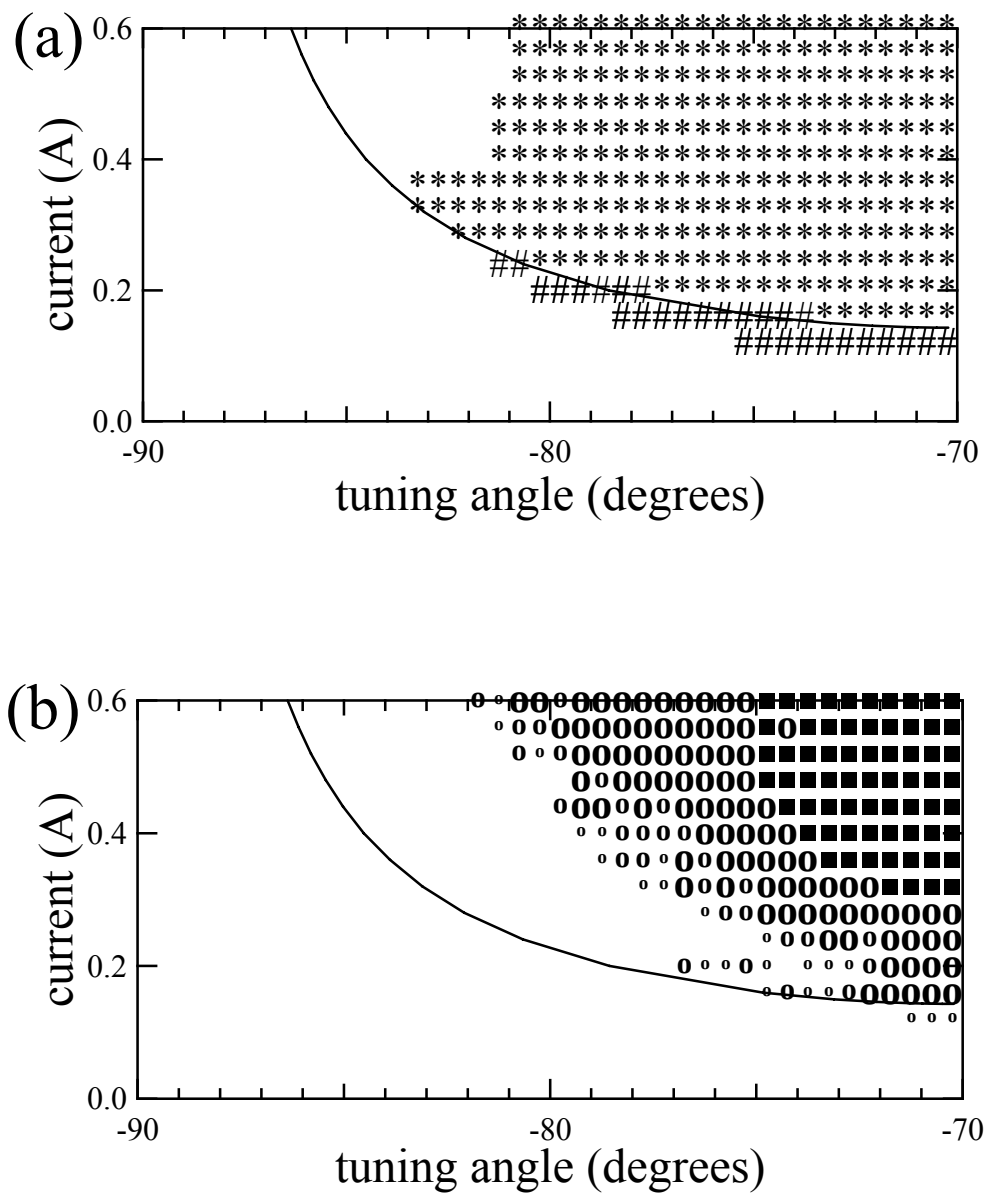

Figure 6. Modeling of a 100-MHz/500-MHz RF system. A solid curve shows the parameters for optimal bunchlengthening. (a) Analytic predictions for no higher order modes. |: coupled-dipole Robinson instability; *: coupled-quadrupole Robinson instability; #: fast dipole-quadrupole Robinson mode-coupling instability; c: coupled-bunch instability with longitudinal mode number of ±1, ±2, or ±3. (b) Results of 500,000-turn simulations of 1440 macroparticles. ₒ : mild instability, where the energy spread exceeds its natural value by 10–30%; **o**: moderate instability, where the energy spread has increased by 30–100%; **O**: strong instability, where the energy spread has increased more than 100%; ■: lost macroparticles.

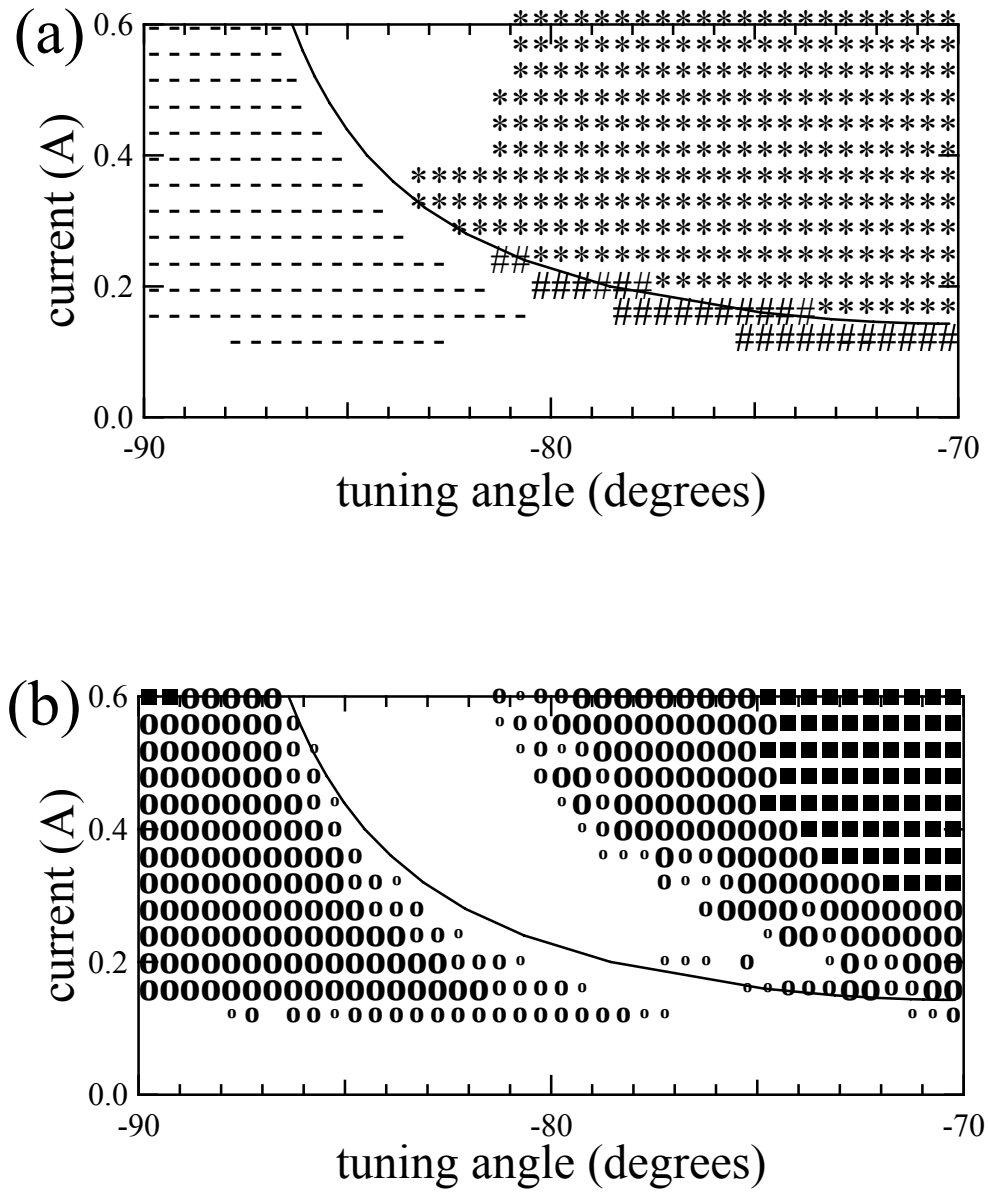

Figure 7. Modeling of a 100-MHz/500-MHz RF system with worst-case parasitic coupled bunch instability. (a) Analytic predictions. –: parasitic coupled bunch instability; |: coupled-dipole Robinson instability; *: coupled-quadrupole Robinson instability; #: fast dipole-quadrupole Robinson mode-coupling instability; c: coupled-bunch instability with longitudinal mode number of ±1, ±2, or ±3. (b) Results of 500,000-turn simulations of 1440 macroparticles. **o** : mild instability, where the energy spread exceeds its natural value by 10–30%; **o**: moderate instability, where the energy spread has increased by 30–100%; **O**: strong instability, where the energy spread has increased more than 100%; ■: lost macroparticles.

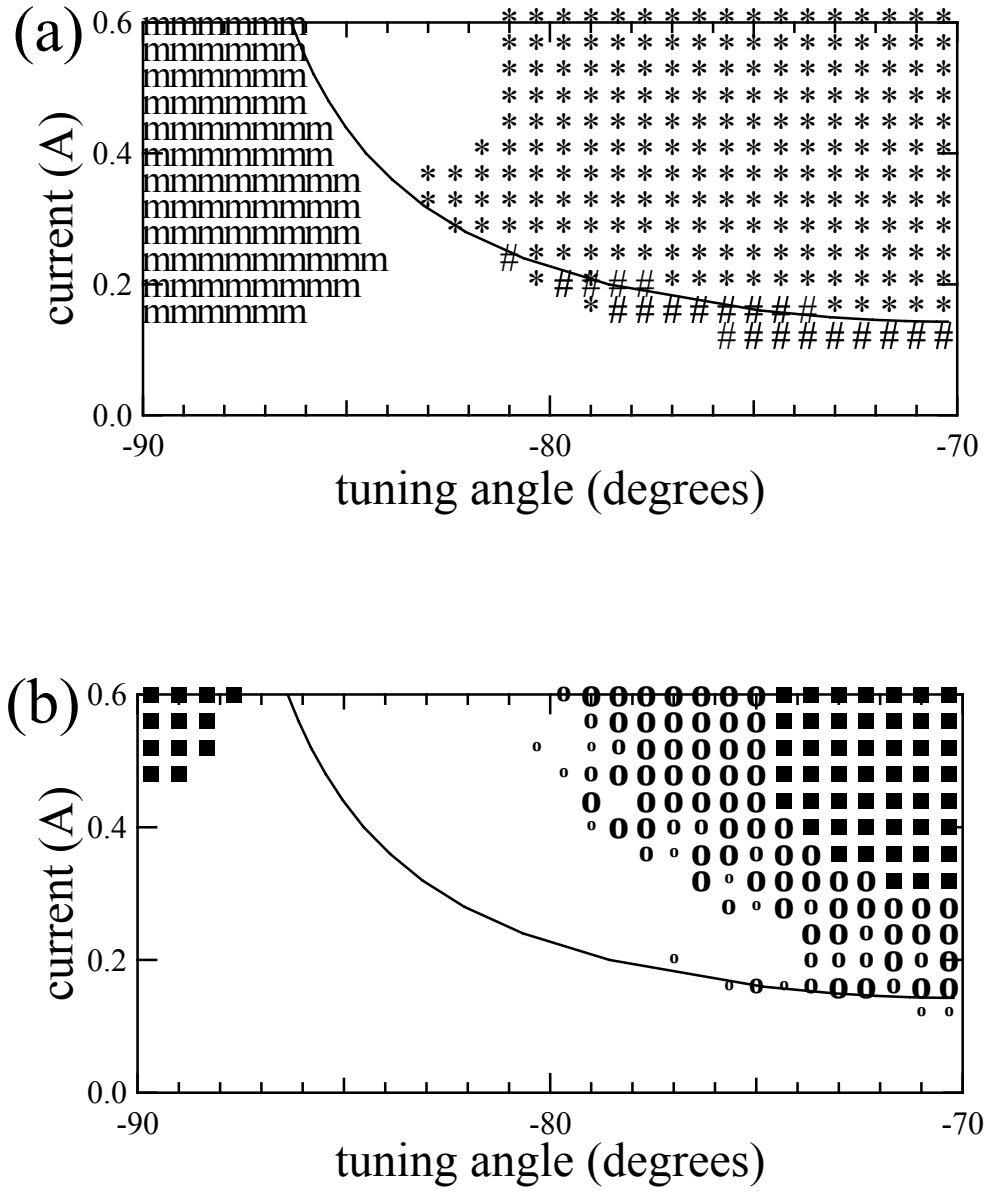

Figure 8. Modeling of a 100-MHz/500-MHz RF system with microwave instability from the broadband impedance $|Z_p/p| = 0.5\ \Omega$. (a) Analytic predictions. m: microwave instability; |: coupled-dipole Robinson instability; *: coupled-quadrupole Robinson instability; #: fast dipole-quadrupole Robinson mode-coupling instability; c: coupled-bunch instability with longitudinal mode number of ±1, ±2, or ±3. (b) Results of 200,000-turn simulations of 288,000 macroparticles. **o** : mild instability, where the energy spread exceeds its natural value by 10–30%; **o**: moderate instability, where the energy spread has increased by 30–100%; **O**: strong instability, where the energy spread has increased more than 100%; ■: lost macroparticles.

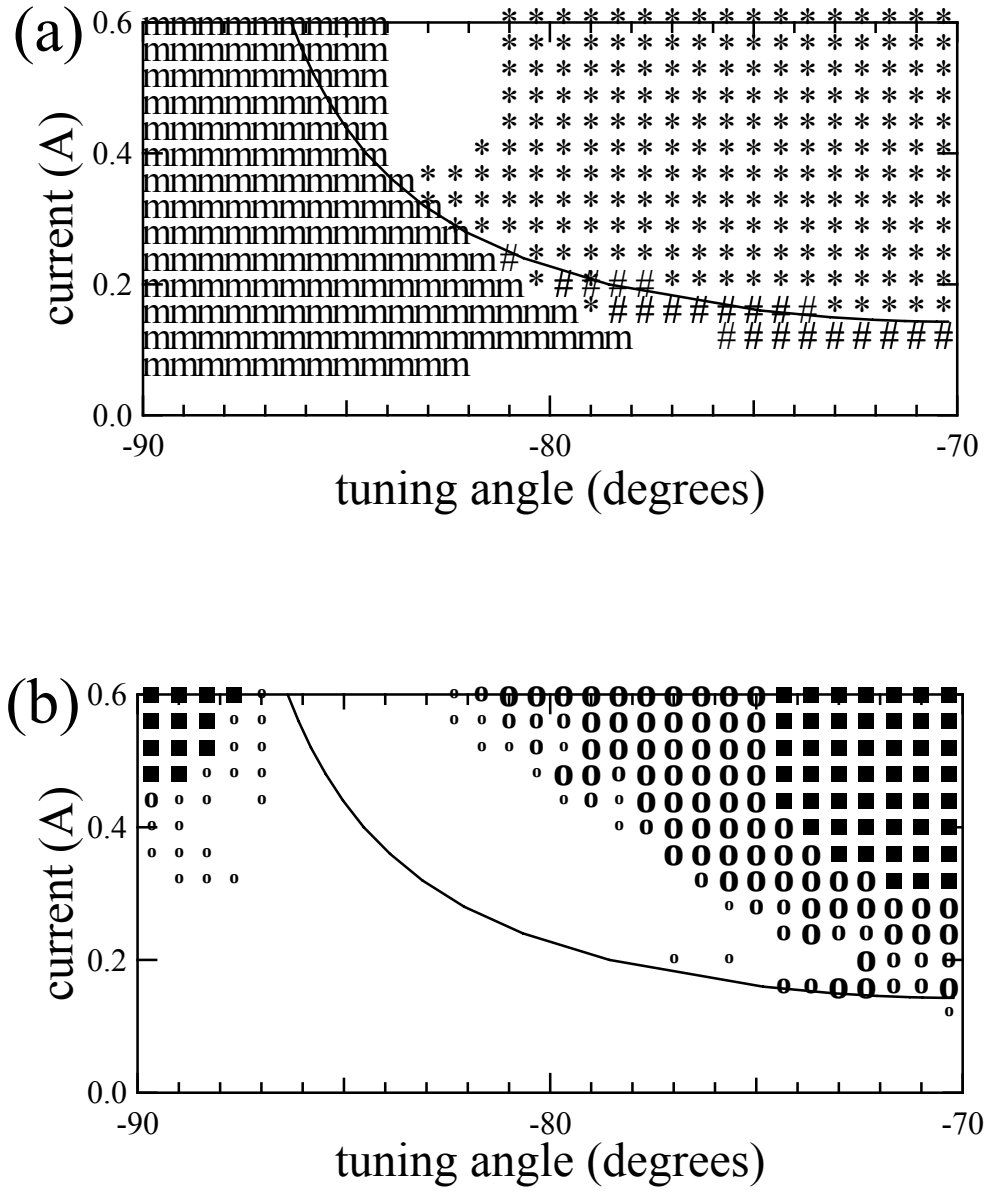

Figure 9. Modeling of a 100-MHz/500-MHz RF system with microwave instability from the broadband impedance $|Z_p/p| = 1\ \Omega$. (a) Analytic predictions. m: microwave instability; |: coupled-dipole Robinson instability; *: coupled-quadrupole Robinson instability; #: fast dipole-quadrupole Robinson mode-coupling instability; c: coupled-bunch instability with longitudinal mode number of ±1, ±2, or ±3. (b) Results of 200,000-turn simulations of 288,000 macroparticles. **o** : mild instability, where the energy spread exceeds its natural value by 10–30%; **o**: moderate instability, where the energy spread has increased by 30–100%; **O**: strong instability, where the energy spread has increased more than 100%; ■: lost macroparticles.

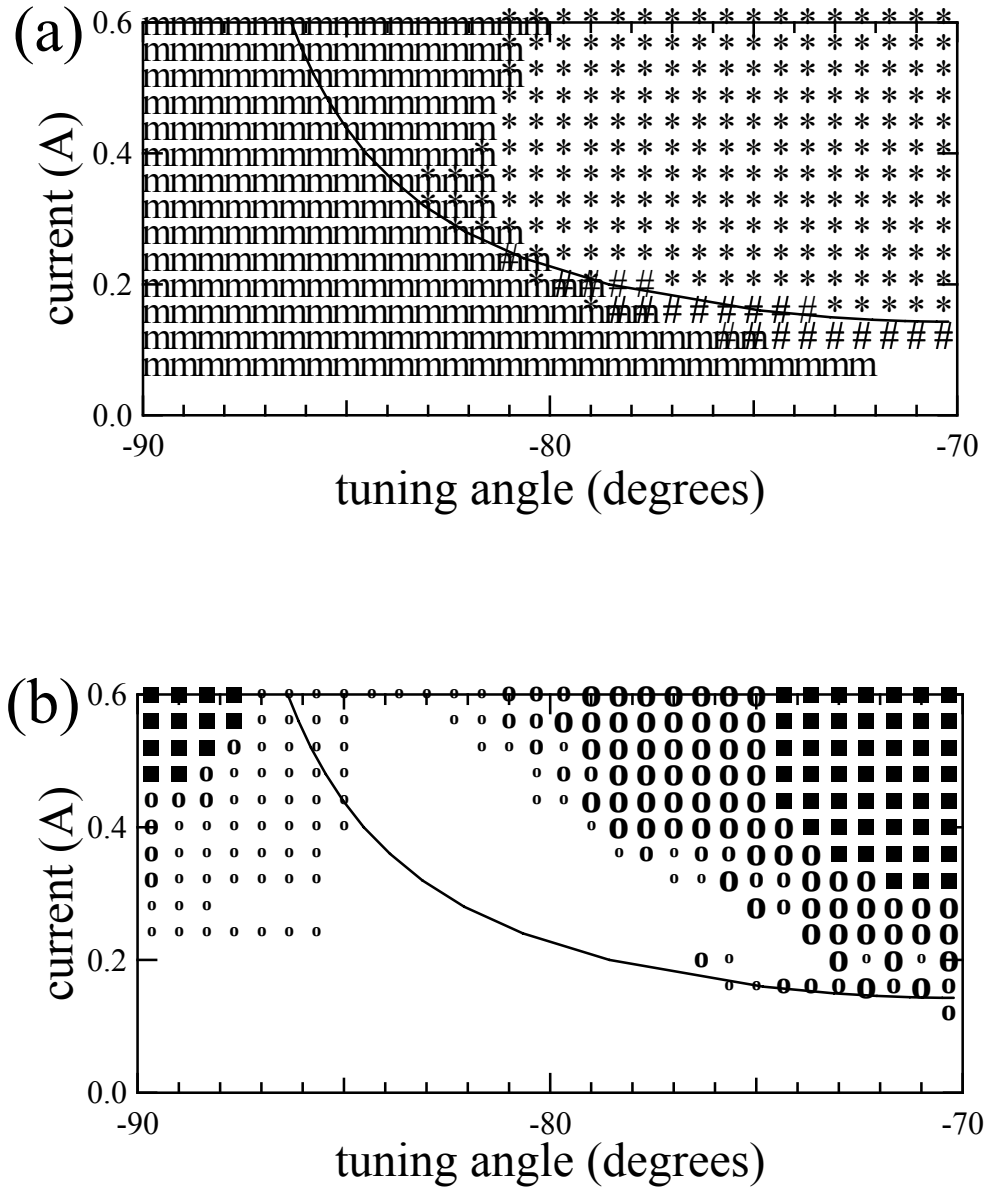

Figure 10. Modeling of a 100-MHz/500-MHz RF system with microwave instability from the broadband impedance $|Z_p/p| = 1.5\ \Omega$. (a) Analytic predictions. m: microwave instability; |: coupled-dipole Robinson instability; *: coupled-quadrupole Robinson instability; #: fast dipole-quadrupole Robinson mode-coupling instability; c: coupled-bunch instability with longitudinal mode number of ±1, ±2, or ±3. (b) Results of 200,000-turn simulations of 288,000 macroparticles. **o** : mild instability, where the energy spread exceeds its natural value by 10–30%; **o**: moderate instability, where the energy spread has increased by 30–100%; **O**: strong instability, where the energy spread has increased more than 100%; ■: lost macroparticles.

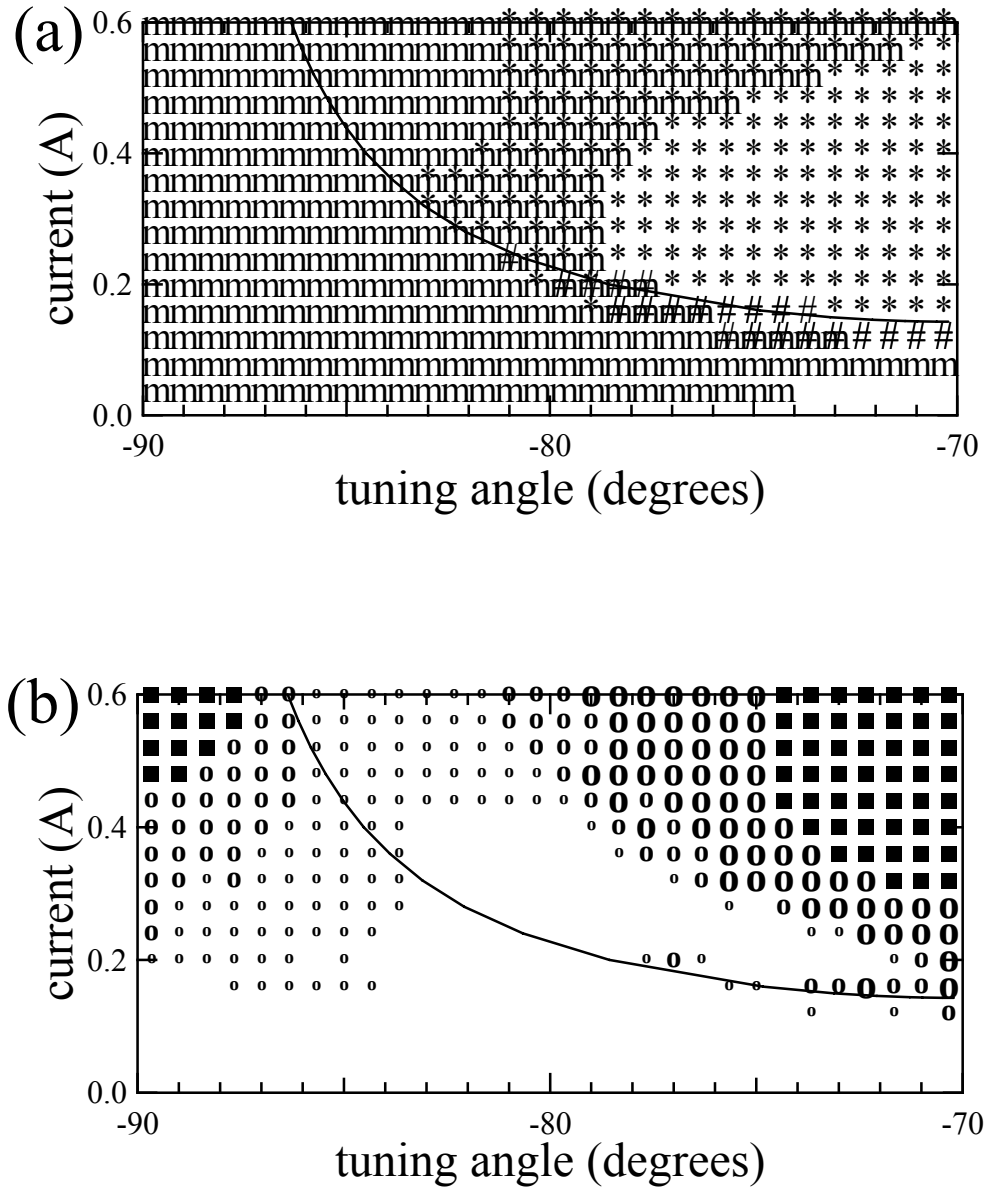

Figure 11. Modeling of a 100-MHz/500-MHz RF system with microwave instability from the broadband impedance $|Z_p/p| = 2\ \Omega$. (a) Analytic predictions. m: microwave instability; |: coupled-dipole Robinson instability; *: coupled-quadrupole Robinson instability; #: fast dipole-quadrupole Robinson mode-coupling instability; c: coupled-bunch instability with longitudinal mode number of ±1, ±2, or ±3. (b) Results of 200,000-turn simulations of 288,000 macroparticles. **o** : mild instability, where the energy spread exceeds its natural value by 10–30%; **o**: moderate instability, where the energy spread has increased by 30–100%; **O**: strong instability, where the energy spread has increased more than 100%; ■: lost macroparticles.

Appendix A. MAD file for the MAX-IV lattice.

```
title, "MAX IV "
FS:      DRIFT,         L=2.3
SS2:     DRIFT,         L=0.5
SS1:     DRIFT,         L=0.15
SS100:      DRIFT,         L=0.1
SHORTFIT:      DRIFT,         L=1.07
SHORTSTR:      DRIFT,         L=0.5
SOFTDIP: SBEND, L=0.3, ANGLE=0.343774677*raddeg, FINT=0.7, HGAP=0.012
MATDIP:   sBEND,    L=0.448799,ANGLE=2.99159761634303006*raddeg,&
  K1=-1.0821158,  FINT=0.7, HGAP=0.012, &
  e1=2.99159761634303006*raddeg/2., e2=2.99159761634303006*raddeg/2.
UNDIP: sBEND, L=0.897598,ANGLE=4.665856594504873*raddeg, &
  K1=-0.94724119, FINT=0.7,HGAP=0.012, &
  e1=4.665856594504873*raddeg/2., e2=4.665856594504873*raddeg/2.
qfun_half: quadrupole, L=0.075, K1=4.15880476
qfun_sex: multipole, K2L=2.021745*2. ! one-third of QFUN's total sextupole
qfun: line=(qfun_sex,qfun_half,qfun_sex,qfun_half,qfun_sex)  ! quadsext
qfm_half: quadrupole, L=0.1, K1=3.8803582008
qfm_sex: multipole, K2L=-.666666667*2. ! one-third of QFM's total sextupole
qfm: line=(qfm_sex,qfm_half,qfm_sex,qfm_half,qfm_sex) ! quadsext
QDM:   QUADrupole,   L=0.15, K1=-3.2188365507 !, K2=0
SF: sextupole, L=0.1, k2=-91.4446*2.
ML: multipole, K3L=32.*6.
RF: RFCAVITY, L=1.0E-7, VOLT=1.2, HARMON=95, BETRF=1.1&
, SHUNT=9.375, TFILL=75.0
UNITCELL:   LINE= (ML,QFUN,SHORTSTR,SF,SS100,UNDIP,SS100,SF,SHORTSTR,QFUN,ML)
BLS:   LINE=(FS,QFM,ML,SS2,QDM,SS1,SOFTDIP,MATDIP,SS100,SF,SHORTFIT,QFUN,ML)
RING: LINE=(BLS,5*UNITCELL,-BLS)
TOT:  LINE=    (12*RING, RF)
USE, TOT
```

Appendix B. MAD file for the lattice AladdinIV_3.

```
title, "ALADDIN IV -3 "  ! chromaticity is corrected
FS:      DRIFT,          L=2.75
SS2:     DRIFT,          L=0.7
SS1:     DRIFT,          L=0.12
SS100:      DRIFT,          L=0.08
SHORTFIT:      DRIFT,          L=0.856
SHORTSTR:      DRIFT,          L=0.4
SOFTDIP: SBEND, L=0.21, ANGLE=0.343774677*raddeg, FINT=0.7, HGAP=0.012
MATDIP:   sBEND,    L=0.31416,ANGLE=2.99159761634303006*raddeg,&
  K1=-1.45 , FINT=0.7, HGAP=0.012, &
  e1=2.99159761634303006*raddeg/2., e2=2.99159761634303006*raddeg/2.
UNDIP: sBEND, L=1.048,ANGLE=4.665856594504873*raddeg*5./3., &
  K1=-0.88, FINT=0.7,HGAP=0.012, &
  e1=4.665856594504873*5./3.*raddeg/2., e2=4.665856594504873*5./3.*raddeg/2.
qfun_half: quadrupole, L=0.06, K1=6.1
qfun_sex: multipole, K2L= 4.737699   ! one-third of QFUN's total sextupole
qfun: line=(qfun_sex,qfun_half,qfun_sex,qfun_half,qfun_sex)  ! quadsext
qfm_half: quadrupole, L=0.07, K1=5.43
qfm_sex: multipole, K2L= 0. ! one-third of QFM's total sextupole
qfm: line=(qfm_sex,qfm_half,qfm_sex,qfm_half,qfm_sex) ! quadsext
QDM:   QUADrupole,   L=0.12, K1=-4.506 !, K2=0
SD: sextupole, L=0.07, k2= -300.6958
ML: multipole, K3L=0.
RF: RFCAVITY, L=1.0E-7, VOLT=0.350, HARMON=95, BETRF=1.1&
, SHUNT=9.375, TFILL=75.0
UNITCELL:   LINE= (ML,QFUN,SHORTSTR,SD,SS100,UNDIP,SS100,SD,SHORTSTR,QFUN,ML)
BLS:   LINE=(FS,QFM,ML,SS2,QDM,SS1,SOFTDIP,MATDIP,SS100,SD,SHORTFIT,QFUN,ML)
SUPER: LINE=(BLS,3*UNITCELL,-BLS)
RING:  LINE=    (12*SUPER, RF)
return
```

Appendix C. The matching file MATCH4.MAD use to create the MATCH4 lattice.

```
! MAD matching command file MATCH4.MAD

call AladdinIV_3.mad ! Start from new lattice AladdinIV_3

!matdip, k1=-1.5  ! It's already at 1.45
use,ring
cell

! Vary quadrupole strengths
!vary,name=matdip[k1],step=0.0001
vary,name=undip[k1],step=0.0001
vary,name=qdm[k1],step=0.0001
vary,name=qfun_half[k1],step=0.0001
vary,name=qfm_half[k1],step=0.0001

! Vary length of ss2 and shortfit
vary, name = ss2[L], step=0.0001
vary, name = shortfit[L], step=0.0001

! Betatron function constraints:
weight, betx=1.5, bety=1.5 ! betatron function matching weights
constraint,range=FS[2],betx=8.,bety=2.75 ! middle of long straight section
constraint, range = qfun_half[1], betx = 4.
constraint, range = qfun_half[3], betx= 4.
constraint, range = qfun_half[5], betx= 4.
constraint, range = qfun_half[7], betx= 4.
constraint, range = ring, bety<20.
constraint, range=ss100[2]/undip[3], bety<10.
constraint, range=ss100[4]/undip[2], bety>6.
constraint, range=ss100[4]/undip[2], bety<7.

! Dispersion constraints at beginning and ends of unitcell dipoles:
constraint, range=undip[1], dx=0.06
constraint, range=undip[2], dx=0.06
constraint, range=undip[3], dx=0.06
constraint, range=ss100[2], dx=0.06
constraint, range=ss100[4], dx=0.06
constraint, range=ss100[6], dx=0.06
constraint, range=ring, dx > 0.0

level,0
lmdif,calls=1000
endmatch
call emittance.mad ! output lattice properties
return
```

Appendix D. MAD file for the MATCH4 lattice.

```
TITLE &
"ALADDIN IV -3: MATCH4_LATTICE "  ! chromaticity corrected, dqxdex=0
!
! DATE AND TIME:    28/04/04  11.16.07
!
! FILE:             MATCH4_LATTICE.MAD
!
FS: DRIFT, L=2.75
SS2: DRIFT, L=0.556580365452
SS1: DRIFT, L=0.12
SS100: DRIFT, L=0.08
SHORTFIT: DRIFT, L=0.90099118674
SHORTSTR: DRIFT, L=0.4
SOFTDIP: SBEND, L=0.21, ANGLE=0.599999999863E-2, HGAP=0.012, FINT=0.7
MATDIP: SBEND, L=0.31416, ANGLE=0.0522132283, K1=-1.45, E1=0.02610661415, E2=&
0.02610661415, HGAP=0.012, FINT=0.7
UNDIP: SBEND, L=1.048, ANGLE=0.135724266667, K1=-0.946149174062, E1=&
0.067862133333, E2=0.067862133333, HGAP=0.012, FINT=0.7
QFUN_HALF: QUADRUPOLE, L=0.06, K1=6.575674076018
QFUN_SEX: MULTIPOLE, K2L= 5.26979989
QFM_HALF: QUADRUPOLE, L=0.07, K1=6.289819901226
QFM_SEX: MULTIPOLE, K2L=1.2154 ! set for dqxdex = 0
QDM: QUADRUPOLE, L=0.12, K1=-5.06288071298
SD: SEXTUPOLE, L=0.07, K2= -339.798529
ML: MULTIPOLE, K3L=0.0
RF: RFCAVITY, L=0.1E-6, VOLT=1.2, HARMON=72, BETRF=1.1&
, SHUNT=9.375, TFILL=75.0
QFUN: LINE=(QFUN_SEX,QFUN_HALF,QFUN_SEX,QFUN_HALF,QFUN_SEX)
QFM: LINE=(QFM_SEX,QFM_HALF,QFM_SEX,QFM_HALF,QFM_SEX)
UNITCELL: LINE=(ML,QFUN,SHORTSTR,SD,SS100,UNDIP,SS100,SD,SHORTSTR,QFUN,ML)
BLS: LINE=(FS,QFM,ML,SS2,QDM,SS1,SOFTDIP,MATDIP,SS100,SD,SHORTFIT,QFUN,ML)
SUPER: LINE=(BLS,3*UNITCELL,-BLS)
RING: LINE=(12*SUPER,RF)
QX := 22.590878652145
QY := 6.367841469126
QS := 0.237531284548E-2
ALFX := -0.624987575653E-8
ALFY := -0.181861397243E-7
BETX := 8.00015418769
BETY := 2.749345472832
X0 := 0.0
PX0 := 0.0
Y0 := 0.0
PY0 := 0.0
T0 := 0.0
PT0 := 0.0
RETURN
```

Appendix E. Input file for harmonic–cavity modeling of MATCH4 with a parasitic higher-order mode.

```
C data for MATCH4-2.1 GeV, nu=5, 6 fundamental, 2 Landau cavities Bosch 7-16-04
       1.2e6    ! vt1 = Cavity 1 peak voltage (volts)
       2.       ! beta1 = Cav. 1 RF coupling coefficient
       19000.   ! q1o = Cavity 1 quality factor (unloaded)
       10.2e6   ! r1o = Cavity 1 impedance at resonance (unloaded) (ohms) for 6 cavities
       0.       ! loadangle1: generator current lags cavity voltage by loadangle1 (deg)
       0.001066 ! alpha = momentum compaction
       7.171e-7 ! To = recirculation time (s)
       72       ! Nbucket = number of buckets, including empty buckets
       2.1e9    ! Ee = electron energy/charge, i.e. energy in eV
       7.75e-4  ! sigmae = relative energy spread from synchrotron radiation
       231.42e3 ! vs = energy loss/revolution from synchrotron radiation (volts)
       8.75e-3  ! t_L = longitudinal radiation damping time (seconds)
       5        ! nu = Cavity 2 harmonic number
       0.       ! beta2 = Cav. 2 RF coupling coefficient
       24000.   ! q2o = Cavity 2 quality factor (unloaded)
       3.4e6    ! r2o = Cav. 2 resonant impedance (unloaded) for 2 cavities
       3000     ! Q3 = HOM quality factor
       10.e3    ! R3 = HOM impedance (ohms)
       6.282309e9   ! w3 = HOM angular frequency (radian/s)
       0.040    ! imin = minimum ring current to be calculated (A)
       0.600    ! imax = maximum ring current to be calculated (A)
       0.040    ! delta_i = ring current increment between calculations (A)
       -89.75   ! phi2_min = minimum Landau tuning angle to be calculated (degrees)
       -70.     ! phi2_max = maximum Landau tuning angle to be calculated (degrees)
       0.5      ! delta_phi2 = Landau tuning angle increment between calculations (degrees)
       1.       ! damp=1: consider Landau damping of Robinson modes, 0: w/o
       0.       ! t_feedback: dipole-mode damping time (seconds); enter 0. for no feedback
       1        ! Nturn_ebar: number of turns to measure energy offset
       20       ! M = number of macroparticles per bucket
       72       ! Nbunch = number of consecutive buckets in bunch train
       500000   ! Nturn_max = number of turns to track
       100      ! Nturn_write = number of turns between passive_15.for output
```

For modeling without consideration of HOMs, R3 was changed to zero.

For modeling the microwave instability, M = 4000, Nturn_max = 200,000, Q3 = 1, w3 = 3.e10, phi2_min = -89.6667, delta_phi2 = 0.6667. To model $|Z_p/p|$ = 0.5 Ω, R3 equals 1712.5 Ω. To model $|Z_p/p|$ = 1 Ω, R3 equals 3425 Ω. To model $|Z_p/p|$ = 1.5 Ω, R3 equals 5137.5 Ω. To model $|Z_p/p|$ = 2 Ω, R3 equals 6850 Ω.